American Mineralogist, Volume 78, pages 1149–1164, 1993

Single-crystal NMR studies of low-concentration hydrous species in minerals: Grossular garnet

HERMAN CHO*
A. A. Noyes Laboratory of Chemical Physics, California Institute of Technology, Pasadena, California 91125, U.S.A.
GEORGE R. ROSSMAN
Division of Geological and Planetary Sciences, California Institute of Technology, Pasadena, California 91125, U.S.A.

ABSTRACT

A detailed solid-state proton NMR study has been performed on garnets containing low levels of OH (0.2–0.3 wt% as H_2O), including a colorless and a pale orange grossular sample from Asbestos, Quebec, and a colorless grossular sample from Lelatema Hills, Tanzania. Synthetic hydrogrossular powder, $Ca_3Al_2(O_4H_4)_3$, has been investigated as well. The NMR spectra of the three natural crystals have a broad line (40 kHz) with a weak sharper feature superimposed. Multiple-quantum spectra indicate that in the Tanzanian garnet the dominant cluster size is two protons; in the colorless grossular from Asbestos a mixture of two proton and four proton clusters is in evidence; in the hydrogrossular powder, the cluster size is four protons.

Solid echo envelope decay experiments show that for all the natural samples a two-step decay process occurs, implying the existence of two distinct proton environments. The area ratios indicate that the spectrum of each of the natural crystals is dominated by a broad line with a Gaussian shape and a line width that differs from the line width of the synthetic hydrogrossular. In the case of the Tanzanian sample, the broad band constitutes ~85% of the area in the NMR spectrum.

Moment analysis shows that although the synthetic hydrogrossular has an average interproton separation of 2.16 Å in the interacting cluster, it is 1.69 Å in the grossular.

INTRODUCTION

In crystalline silicates, the hydrogarnet substitution $SiO_4^{4-} \leftrightarrow 4OH^-$ has been presumed to be a common and favored form of OH^- substitution, its existence well established in the series grossular-katoite [$Ca_3Al_2(SiO_4)_3$-$Ca_3Al_2(H_4O_4)_3$]. Recent infrared spectral studies of naturally occurring garnets indicate that minor amounts of OH^- commonly occur in macroscopic garnets, but that modes of substitution other than the hydrogarnet substitution are prevalent (Rossman and Aines, 1991). This possibility is reinforced by the NMR studies of Kalinichenko et al. (1987) of polycrystalline hydrogarnet with 3.44 wt% H_2O, which proved that H occurs in the sixfold-coordinated Al site. On the basis of crystallographic studies, others have also concluded that H may possibly occupy sites other than the Si site. (Basso and Cabella, 1990; Birkett and Trzcienski, 1984).

A combination of analytical methods is required to obtain a more complete picture of the identity and structure of hydrous defects in anhydrous minerals. Along with IR absorption spectroscopy, NMR spectroscopy is perhaps one of the most informative options. The principal challenge in the investigation of silicate materials with proton NMR spectroscopy is primarily a technical one, namely, overcoming or accommodating its intrinsically low sensitivity. Many of the most interesting phenomena associated with hydration of silicate minerals are observed at concentrations that test the sensitivity thresholds of the most advanced NMR spectrometers available. Consequently, few NMR studies of hydrous species in minerals have been reported (Yesinowski et al., 1988).

We have attempted to address in this work the dual problems of low H concentration and interference of proton background signals by a number of experimental strategies, and we report the results of NMR investigations on the incorporation of hydrous species at low concentrations on three single-crystal grossular garnet samples and one synthetic hydrogarnet powder. This paper is organized in three parts. First, we present results of holeburning experiments on the three single-crystal grossular samples, which indicate that H nuclei are clustered. Next, we characterize these presumptive clusters through the use of recently developed multiple-quantum NMR methods. We test the reliability of this technique in the context of silicate mineral systems and provide evidence from experiments on a synthetic hydrogrossular powder that this technique can be applied to obtain reliable counts

* Present address: Molecular Science Research Center MSIN K2-20, Pacific Northwest Laboratory, Richland, Washington 99352, U.S.A.

0003–004X/93/1112–1149$02.00

TABLE 1. Descriptions of garnet NMR samples

Material	Hydrogrossular	Grossular		
Locality	Synthetic powder	Lelatema Hills, Tanzania	Jeffrey mine, Asbestos, Quebec, Canada	Asbestos, Quebec, Canada
Color	colorless	colorless	colorless	pale orange
Catalog no.		GRR1386	GRR1537	GRR53
Mass for NMR	189.3 mg	193.6 mg	110.6 mg	264.1 mg
H_2O content*		0.17 wt%	0.27 wt%	0.31 wt%

Compositions

(1) $Ca_3Al_2(O_4H_4)_3$ (Lager et al., 1987)
(2) $Ca_{2.95}Mg_{0.04}Mn_{0.01}Fe_{0.01}Al_{1.97}Ti_{0.02}Si_{2.99}O_{12.00}$ (Gr2 in Shannon and Rossman, 1992)
(3) $Ca_{2.98}Mg_{0.00}Mn_{0.01}Fe_{0.01}Al_{1.97}Ti_{0.00}Si_{2.94}O_{12.00}$ (Gr3 in Shannon and Rossman, 1992)
(4) $Ca_{2.92}Mg_{0.00}Mn_{0.04}Fe_{0.14}Al_{2.00}Ti_{0.00}Si_{3.00}O_{12.00}$ (Gr1 in Shannon and Rossman, 1992)

* OH content, expressed as wt% H_2O, was obtained from the integrated absorbance in the region of 3800–3400 cm^{-1}. The H_2O contents were estimated using a linear fit to the calibration data from Table 3 of Rossman and Aines (1991), which apply to grossular with <0.5 wt% H_2O.

of the number of protons in closely spaced groups of H nuclei. We then proceed to apply this method to the natural garnets to determine the number of H nuclei constituting the clusters at the hydrated sites.

The final part of this paper is an analysis of the NMR line shape of the grossular garnets and a discussion of the information that can be deduced from the spectrum, based on the knowledge gained from the previous experiments.

EXPERIMENTAL

Sample selection and preparation

Descriptions of the samples studied in this work are compiled in Table 1. A primary consideration governing the choice of these samples was the H_2O concentration: for the specific experiments and samples investigated here, we estimate the proton detection threshold to be approximately 10^{17} H nuclei in the solid state, with a maximum sample volume of 0.5 cc.

The single crystals were judged by several other criteria: freedom from cracks, twinning, and visible inclusions (as determined by examination at 40× magnification) and concentration of paramagnetic and ferromagnetic impurities. Specimens with the fewest crystal defects and lowest concentrations of paramagnetic and ferromagnetic impurities were deemed the most desirable for investigation by NMR.

Single-crystal specimens were prepared for the NMR experiments by immersing in acetone, wiping with paper tissue, and drying with a heat gun. The crystals were cleaned two or more times afterward by a similar procedure, but with spectral grade carbon tetrachloride as the solvent. After the final cleaning, the crystals were stored under 0.1-torr vacuum at 100 °C for 20 h and then wrapped in small amounts of Teflon tape to prevent movement of the sample while positioned inside the NMR coil. The Teflon tape was checked for H content by scanning the proton NMR resonance of several strips randomly taken from different rolls of tape. None was found to contain amounts of H detectable by NMR at room temperature, even after several thousand scans.

All cleaned samples were handled with latex gloves and clean metal instruments only, to protect against contamination of the crystal surface by H-containing residue. The Teflon-wrapped samples were periodically unwrapped and rewrapped with new tape to ensure the cleanliness of the outer surface for experiments lasting several days.

NMR experiments

General remarks. NMR experiments were performed at room temperature in a 4.7-T magnetic field, corresponding to a proton Larmor frequency of 200.135 MHz. The radio frequency pulse times and phases were adjusted by standard multiple-pulse calibration techniques on a large H_2O sample sealed inside a glass tube (Burum et al., 1981). The >130 kHz radio frequency field generated by our NMR probe sufficed to ensure the uniform excitation of the entire spectral range of all samples in Table 1.

The near ubiquity of H was a significant complication attending our efforts to observe proton NMR signals from samples with low H content. To accomplish the isolation of the sample from H-containing contaminants, we have constructed a customized NMR probe, with its coil suspended on top of two Cu rods approximately 2 cm above a Teflon base. The Teflon base, although not free of H, did not produce a measurable background signal in the NMR spectrum. This base and the Teflon dielectric jacketing the coaxial cable conducting radio frequency current to the coil were the only nonmetallic parts within 6 cm of the sample. The NMR coil, which was wound from a strip cut from an unvarnished Cu sheet, was washed by repeated immersion in concentrated HCl or carbon tetrachloride, followed by drying with a heat gun. The coil was attached to the Cu rods by minimal amounts of solder and then sprayed and wiped with solder flux remover and carbon tetrachloride.

To reduce the signal originating from humidity in the atmosphere, the bore of the superconducting magnet was sealed at both ends, except for a small outlet at the bottom, and the air within purged by directing high-pressure, dried, filtered air through a transfer tube directly onto the sample and out the exhaust port.

In addition to the above measures, every NMR experiment on the grossular garnets was performed twice under identical conditions, once with the sample loaded in the probe and once without. The NMR signal of the sample was thus obtained by forming the difference of the two experimental signals.

Multiple-quantum NMR experiments. Procedures for generating and detecting multiple-quantum spin coherences in a two-dimensional NMR experiment have been recently documented (Weitekamp, 1983; Munowitz and Pines, 1987). We have utilized versions of the two-D

multiple-quantum experiment wherein the mixing period was a phase-shifted, time-reversed counterpart of the preparation period and the evolution period was omitted. The different multiple-quantum orders were resolved by incrementing the phase of the preparation period from acquisition to acquisition and keeping the evolution period equal to zero throughout, in the manner described by Shykind et al. (1988). The incremented phase shifts of the preparation period were implemented by inserting a composite z pulse (Freeman et al., 1981) between the preparation period and mixing periods of the multiple-quantum pulse sequence, as illustrated in Figure 1a and 1b. The problems arising from the sensitivity of this method to radio frequency field heterogeneity were minimized by employing NMR coils with inner volumes several times larger than the volume of the samples. We have verified that the radio frequency homogeneity was adequate for these experiments by monitoring the Rabi oscillations (Abragam, 1961) of an adamantane powder sample over several periods and by performing multiple-quantum measurements on solid samples having known high maximum multiple-quantum transition orders.

Nonselective multiple-quantum spectra were acquired with the use of the one-quantum pulse sequence of Suter et al. (1987), whereas even-order selective spectra were acquired with the even-quantum pulse sequence developed by Warren et al. (1980). A typical time for one cycle of these excitation sequences was 60 μs.

A delay of 10 ms was inserted after the mixing period to permit the irreversible decay of spin order not aligned along the axis of quantization. This time was short compared with spin-lattice relaxation times, but long relative to the time constant of the sample's free induction decay (FID) transient. The remaining longitudinal magnetization was sampled by means of a pulsed spinlock train (Ostroff and Waugh, 1966), with acquisition of data occurring between spinlock pulses. Radio frequency pulses corresponding to an approximately $\pi/4$ flip angle were utilized in the spinlock train (Rhim et al., 1976), spaced by 19-μs intervals, and 4096 complex spinlock points were acquired in these experiments. An eight-step phase cycle of the detection-period pulses was implemented to reduce artifacts induced by the receiver and flip angle.

Detector and filter ringing due to pulse breakthrough during the spinlock detection period was attenuated through the placement of a blanking switch on the input of the NMR receiver. Because of the reduction of pulse breakthrough, the signal-to-noise ratio could be further improved by using narrower filter band widths than would otherwise be practical in a multiple-pulse NMR experiment. In these experiments, we have set the filter width to be approximately the inverse of the separation between spinlock pulses.

Two complete periods of the multiple-quantum interferograms were acquired in all multiple-quantum NMR experiments recounted here. The data were analyzed by adding the 4096 complex points in the summed spinlock transient for each value of the phase increment individually, Fourier transforming the complex interferogram with respect to the phase variable, and then computing the magnitude spectrum. The positive and negative order intensities of spectra computed in this way represent uncorrelated measurements and were both used in the least-squares fits to be discussed later.

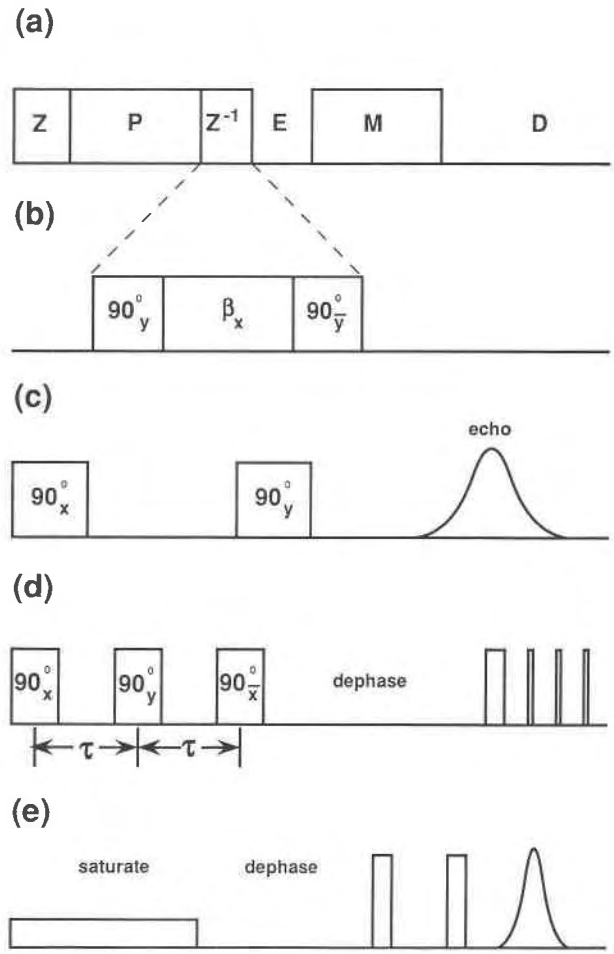

Fig. 1. Pulse sequences of the NMR experiments discussed in this paper. (**a**) Generic multiple-quantum NMR experiment, composed of preparation (P), evolution (E), mixing (M), and detection (D) intervals; (**b**) composite z pulse constructed from a sandwich of three pulses with standard quadrature phases; (**c**) two-pulse solid echo sequence; (**d**) pulse sequence for measuring solid echo envelope decays by pulsed spinlock detection; (**e**) hole-burning experiment with two-pulse solid echo detection.

Spin echo and solid echo envelope decay experiments. The garnet NMR spectra were recorded with the standard solid echo sequence shown in Figure 1c (Powles and Strange, 1963). The phases of the pulses and receiver were iterated through a 16-step phase cycle designed to eliminate receiver and pulse artifacts. The refocusing time for these experiments was chosen to be 20 μs, although different values were explored to verify that the areas and line widths of the garnet spectra were independent of τ.

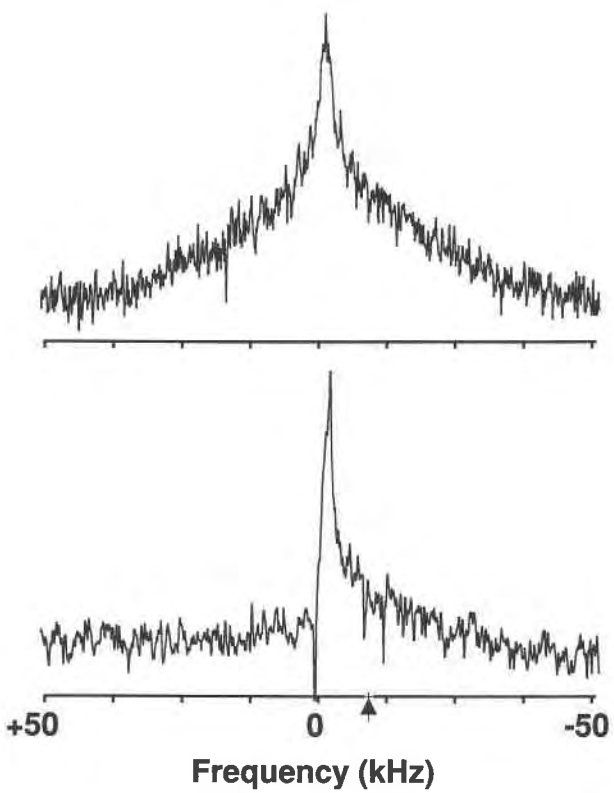

Fig. 2. Proton NMR spectra of the Tanzanian grossular garnet both (**top**) without and (**bottom**) with a hole-burning field. The carrier frequency of the hole-burning field is marked by the arrow on the horizontal axis. Both spectra are the averages of 2000 scans with a 4-s delay between scans and are plotted with equal vertical scaling.

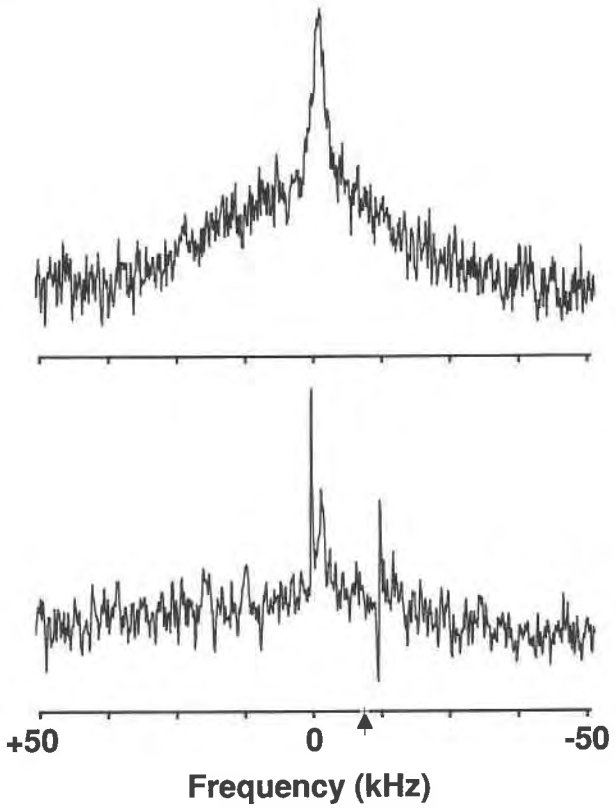

Fig. 3. Same as Fig. 2, but for the colorless grossular from the Jeffrey quarry, Asbestos, Quebec.

The τ independence of our results was affirmed for $\tau >$ 12 μs.

The solid echo envelope experiment depicted in Figure 1d is a version of the standard experiment, modified by us to increase its sensitivity. The modification consists of measuring the echo amplitude with a pulsed spinlock train, as described in the previous section, rather than by its refocused free induction decay. The enhancement of the signal-to-noise ratio depends on the $T_{1\rho}$ of the sample and the recovery time of the detector and tank circuit, but in favorable cases it can be several orders of magnitude.

Results and discussion

NMR spectra: Homogeneous vs. heterogeneous broadening

Spectra were recorded for at least three random orientations of each of the single-crystal grossular samples, using the two-pulse solid echo sequence diagrammed in Figure 1c. Representative spectra for all three samples are pictured in Figures 2a, 3a, and 4a. To within the resolution of the experiment, the appearance of the NMR spectrum for each crystal was not altered by changes in the orientation of the crystal with respect to the direction of the static magnetic field. More detailed analyses of these spectra (discussed below) confirm this assessment quantitatively. As a result of this apparent orientation independence, no measures were taken to position the crystals in special, known orientations for any of the NMR experiments described below.

The NMR spectra for all three samples appear to consist of two distinct lines, one broad line approximately 40 kHz full width at half height (FWHH), and one narrow line superimposed on the broader peak and with approximately the same center frequency. The observation of the broad line indicates immediately the existence of fixed or slow-moving H clusters in the crystal, since broad lines in proton spectra are usually the consequence of short-range homonuclear dipolar couplings (Abragam, 1961). Nevertheless, other sources of line broadening not involving H clustering could plausibly account for the observed line shape as well. Chief among these is the presence in all three samples of trace amounts of paramagnetic ions and an unknown number of crystal lattice defect sites. The heterogeneity of magnetic environments for individual protons can give rise to line broadening in this situation by creating a heterogeneous distribution of proton resonances, with a concomitantly broad NMR line shape.

To decide which of these two mechanisms is respon-

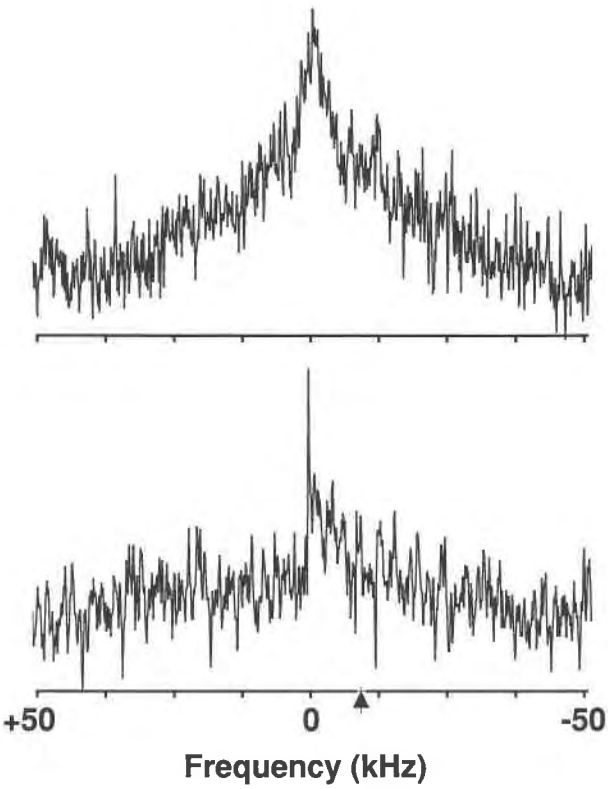

Fig. 4. Same as Fig. 2, but for the orange grossular from Asbestos, Quebec.

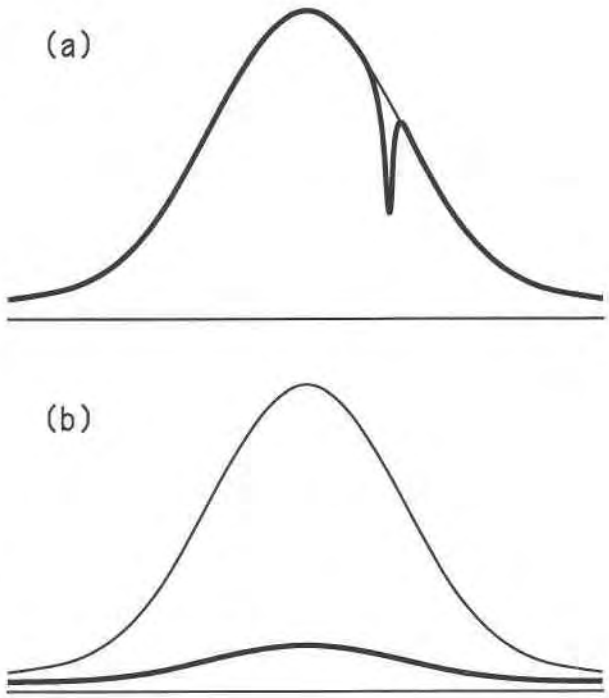

Fig. 5. Possible responses of a wide NMR line to a weak hole-burning field for the cases where the line width is due to (**a**) heterogeneous line broadening interactions, and (**b**) homogeneous line broadening mechanisms. The narrow line represents the unperturbed line shape, the bold line the line shape after irradiation with a hole-burning field.

sible for the shape of the proton line, the hole-burning experiment sketched in Figure 1e was carried out on the grossular single crystals (Mehring, 1983). The predicted responses to a hole-burning field for the case of heterogeneous broadening and the case of homogeneous broadening are depicted in Figure 5a and 5b, respectively.

The results of the hole-burning experiments are displayed in Figures 2b, 3b, and 4b. The rotating frame amplitude of the saturating field in these experiments was estimated to be approximately 4 kHz, a value that adequately fulfills the condition that the excitation range of the weak pulse be narrow, compared with the line width of the resonance. A dephasing interval 10 ms in duration was inserted after the weak rf pulse to allow residual transverse magnetization to decay before acquisition of the echo. This interval, although long compared with the T_2 for the samples, was short compared with the T_1 (>1 s at room temperature). The duration of the weak rf pulse for these experiments was 10 ms.

The spectra show that almost the entire broad feature disappears as a result of the irradiation with the weak field. We conclude on the basis of this result that the line width is not due to heterogeneous distribution of narrow spectral packets but is more likely attributable to homogeneous interactions, such as homonuclear dipolar couplings of clustered protons.

Multiple-quantum NMR

Application to cluster size determination. The results of the previous section indicate that H nuclei in the three grossular samples probably exist in the form of closely spaced groups of protons, with interproton separations within a group of no more than a few ångströms, as inferred from the roughly 1-mT width of the broad proton line. To gain further insight into the size, arrangement, and identity of these clusters, we performed the multiple-quantum NMR counting experiment illustrated in Figure 1a (Baum and Pines, 1986; Baum et al., 1985). The procedure for determining cluster sizes by multiple-quantum NMR methods consists of fitting multiple-quantum spectra to known equations relating cluster size to multiple-quantum line intensities. If we adopt certain assumptions about multiple-quantum transition probabilities, the integrated intensity of the $\pm\Delta m$ quantum line can be derived by a simplified combinatorial argument (Hoffman, 1970; Wokaun and Ernst, 1978). This formula is given by the expression

$$I(\pm m) = \frac{(2N)!}{(N-m)!(N+m)!} \quad (1)$$

where N is the putative number of coupled-spin ½ nuclei. The reliability of this formula has been empirically con-

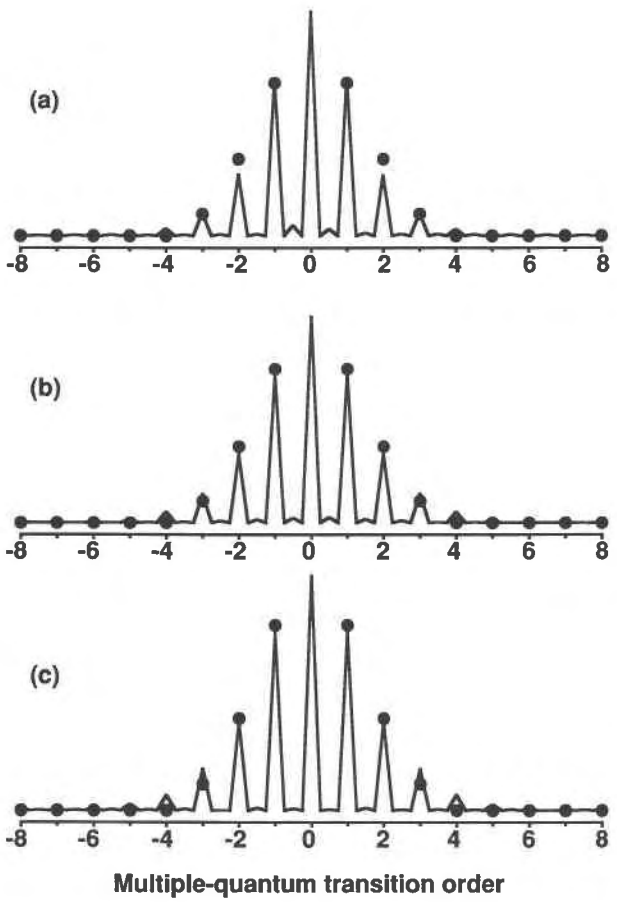

Fig. 6. Multiple-quantum NMR magnitude spectra of the synthetic hydrogarnet powder for preparation periods of duration (a) 240 μs (four cycles); (b) 360 μs (six cycles); and (c) 600 μs (ten cycles). The solid circles represent least-squares fits of the multiple-quantum line intensities to Eq. 1 and indicate a proton cluster size of four. Each phase increment point in the experiment corresponds to the sum of 40 scans of 4096 complex spin-lock points each, with a recycle delay between scans of 4 s.

firmed in previous experiments (Baum and Pines, 1986; Baum et al., 1985).

For more general systems containing noninteracting clusters of more than one size, Equation 1 can be modified in the following way:

$$I(\pm m) = A_0 + \sum_{j=1}^{L} A_j \frac{(2N_j)!}{(N_j - m)!(N_j + m)!} \qquad (2)$$

where the A_j represent the relative contribution of the jth cluster to the total intensity observed at a given m value, and L is the number of cluster sizes present.

Although Equations 1 and 2 contain no reference to the properties of the spin system other than the cluster size, or to the specific details of the multiple-quantum experiment used to obtain the spectrum, the intensities can in fact depend very strongly on a number of other parameters, most notably on the duration of the interval known as the preparation period. The multiple-quantum experiments attempted in this work were therefore performed several times, with successively longer preparation periods for each repetition. Convergence to the statistically determined limit was decided when the fitted cluster size inferred from the spectrum ceased to increase as the preparation time was lengthened.

Synthetic hydrogarnet powder multiple-quantum results. Multiple-quantum spectra of the synthetic hydrogarnet powder for three preparation times are displayed in Figure 6, accompanied by solid circles denoting the nonlinear least-squares fit of the experimental intensities to the single cluster intensity formula in Equation 1. The nonselective pulse sequence described in the experimental section was employed during the preparation and mixing periods to generate the multiple-quantum spin coherences. Because of the unique susceptibility of the zero quantum line to errors from experimental artifacts and instrumental instabilities, the intensity of this line only was excluded from the calculation of the fit. The computer program employed to fit these data incorporates a table containing information on the maximum coherence orders admissible for spin clusters of a given size N, thus ensuring that the physical limits on the largest multiple-quantum transitions observable in clusters of finite size are recognized by the fitting program. The value of N that best satisfied the least-squares criterion was determined to be four for every spectrum, signifying that the statistical limit has indeed been reached, and that the system's predominant cluster consists of four H nuclei. In view of previous independent work showing that H nuclei are grouped in clusters of $(OH)_4$ tetrahedra (Cohen-Addad et al., 1967), the determination of a H cluster size of four validates the reliability of multiple-quantum NMR as a method for counting clustered H nuclei in garnets.

Despite the goodness of fit of the experimental spectra to Equation 1 for $N = 4$, the finding that the hydrogarnet cluster size is four is contradicted by the presence of clearly visible 4- and 5-quantum lines in Figure 6c. As demonstrated in the appendix, all multiple-quantum transitions involving $|\Delta m| \geq 4$ are forbidden in clusters with $N = 4$ for this particular version of the multiple-quantum experiment. The fact that these higher order transitions are observed implies that the $(OH)_4$ tetrahedra cannot be regarded as truly isolated in the NMR sense, and that a residual magnetic coupling does exist between at least some of the tetrahedra. Inasmuch as the dipolar coupling is a function of the interproton vector and the direction of the magnetic field (Abragam, 1961), the magnitude of the intercluster coupling depends both on the position of the tetrahedron within the structure and on the orientation of the individual crystallites constituting the powder. In this and other cases, the least-squares fit becomes critical for extracting the most probable cluster size from the experimental intensities.

Tanzanian garnet multiple-quantum results. The same multiple-quantum experiment performed on the hydrogarnet in the previous section was carried out on a sample consisting of two Tanzanian garnet single crystals with a

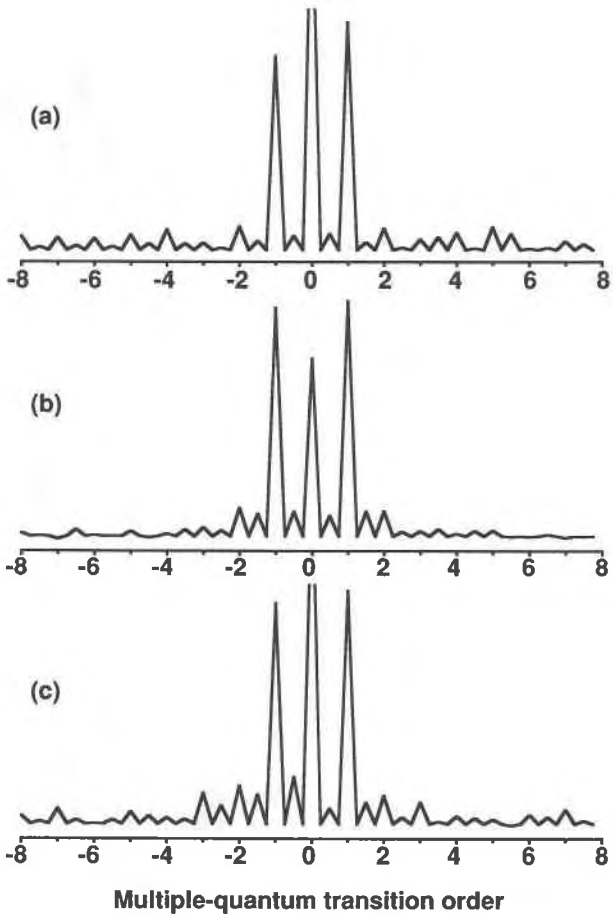

Fig. 7. Multiple-quantum NMR magnitude spectra of the Tanzanian grossular garnet for preparation periods of duration (**a**) 240 μs (four cycles); (**b**) 480 μs (eight cycles); and (**c**) 720 μs (12 cycles). Each phase increment point in the experiment is the sum of 560 scans of 4096 complex spinlock points each, with a recycle delay per scan of 4 s.

combined mass of 646.1 mg. Three spectra corresponding to three different preparation times were recorded in this manner, with the results shown in Figure 7.

Unlike the spectra for the synthetic hydrogarnet powder, in the multiple-quantum spectra of the grossular single crystals only the $\Delta m = \pm 1$ quantum lines have appreciable intensity. For reasons given in the appendix, we conclude that the number of clustered H nuclei revealed by these data must be greater than or equal to two. Moreover, if we accept the validity of Equation 1, then we find that the ratio of the ± 2 quantum transition intensity to the ± 1 quantum transition intensity for cluster sizes $N \geq 3$ must satisfy the inequality

$$I(\pm 2)/I(\pm 1) \geq \tfrac{2}{5}. \quad (3)$$

It is clear from the signal-to-noise ratio of all three spectra that ± 2 quantum lines 40% as intense as the ± 1 quantum lines would readily be detectable if they were present. Since these lines are evidently absent, we infer that N must be two.

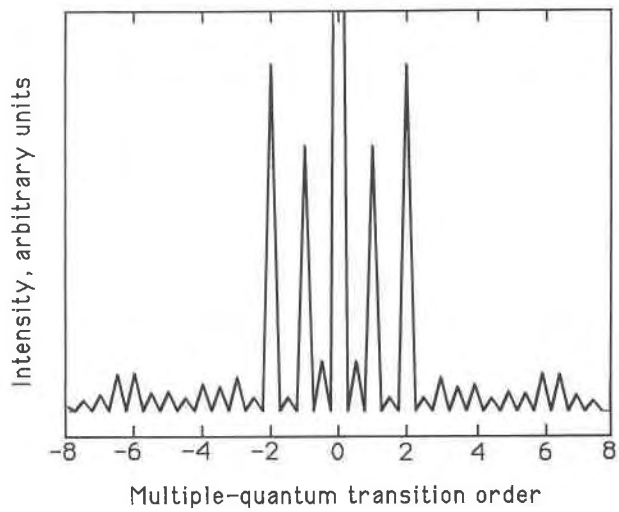

Fig. 8. Even-order selective multiple-quantum NMR magnitude spectrum of the Tanzanian garnet for a preparation period of 240 μs. The points in the interferogram are the sum of 400 scans of 4096 complex spinlock points each, with a recycle delay of 4 s per scan.

Additional support for this assertion is provided by the multiple-quantum spectrum shown in Figure 8. The even-order selective multiple-pulse sequence used in the preparation period of this experiment preferentially populates the even-quantum coherences in the spin system, and so intensities of even order transitions are enhanced in the spectrum and those of odd order transitions suppressed. For this experiment, the ± 2 quantum transitions of clusters consisting of just two H nuclei have nonzero intensities. The observation of the ± 2 quantum lines in this spectrum therefore lends credence to the claim that H nuclei exist primarily as discrete, closely spaced pairs in the garnet crystal structure.

The NMR spectrum of isolated pairs of magnetically equivalent protons has a readily identified form for rigid solids (Pake, 1948). No such pattern can be discerned in the spectrum of the Tanzanian grossular in Figure 2a. Two inferences may tentatively be drawn from this observation. The first is that the two protons constituting a garnet pair are probably not magnetically equivalent nor well isolated from interactions with other magnetic isotopes such as ^{27}Al or ^{29}Si. When the effects of chemical shift anisotropy and orientational averaging are also taken into account, the NMR spectrum of the proton pairs could come to resemble more closely the spectrum of Figure 2a.

The second inference to be made from these results is that proton pairs may occur in a variety of magnetically inequivalent orientations within the crystal. The complexity of the unit cell, with numerous locations where proton pairs could conceivably be situated, supports this conjecture (Novak and Gibbs, 1971). The orientation independence of the NMR spectrum provides additional evidence for this supposition. The NMR spectrum for

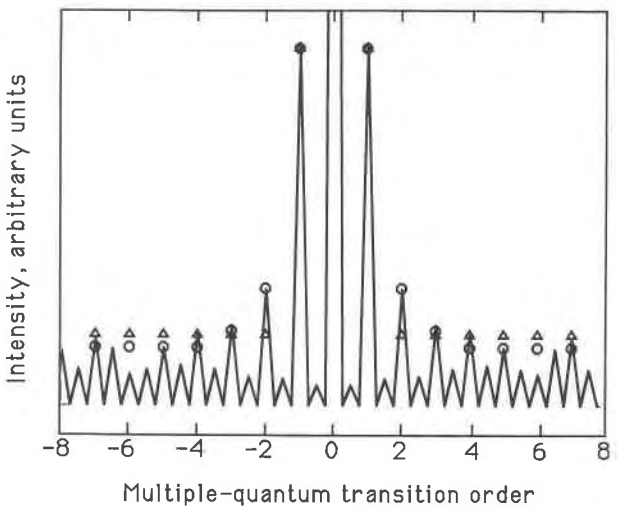

Fig. 9. Multiple-quantum NMR magnitude spectrum of the colorless grossular (GRR 1537) from the Jeffrey quarry for a preparation period of 240 μs. The spectrum was symmetrized by zeroing the imaginary buffer prior to Fourier transformation; 560 scans of 4096 complex spinlock points each were acquired and summed per phase increment, with a recycle delay of 4 s per scan. The triangles symbolize the least-squares fit of a single cluster model to the experimental intensities (cluster size = 2), and the circles the fit of a two cluster model to the experimental data (cluster sizes = 2, 4).

this case would be a superposition of appropriately weighted multiplets, with each multiplet having different splittings and center frequencies depending on the direction of the interproton vector, the magnetic field, and the orientation of the crystal.

Asbestos garnet multiple-quantum results. The multiple-quantum spectrum for the garnet from the Jeffrey quarry (GRR 1537) appears in Figure 9. The small number of H nuclei in the crystal made observation of the multiple-quantum signal difficult in this sample, as manifested by the poor signal-to-noise ratio. Consequently, our determination of the H cluster size from this spectrum is extremely uncertain.

The only peaks in the spectrum that we can confidently identify are the ± 1 quantum lines. However, weak ± 2 quantum lines are visible above the noise as well. We have performed nonlinear least-squares fits of the experimental intensities to Equation 2 for $L = 1$ (one cluster), and $L = 2$ (two clusters). The best one-cluster model fit, represented by the triangles, is obtained for a cluster size of two. For the two-cluster model, the best least-squares fit is obtained for clusters of size two and four. The fitted equation for the two-cluster model contains more adjustable parameters than the corresponding equation for the one-cluster model, and thus more accurately fits the data. Statistical tests we have performed that account for this bias, however, verify that the two-cluster equation does in fact provide a superior fit to the experimental intensities.

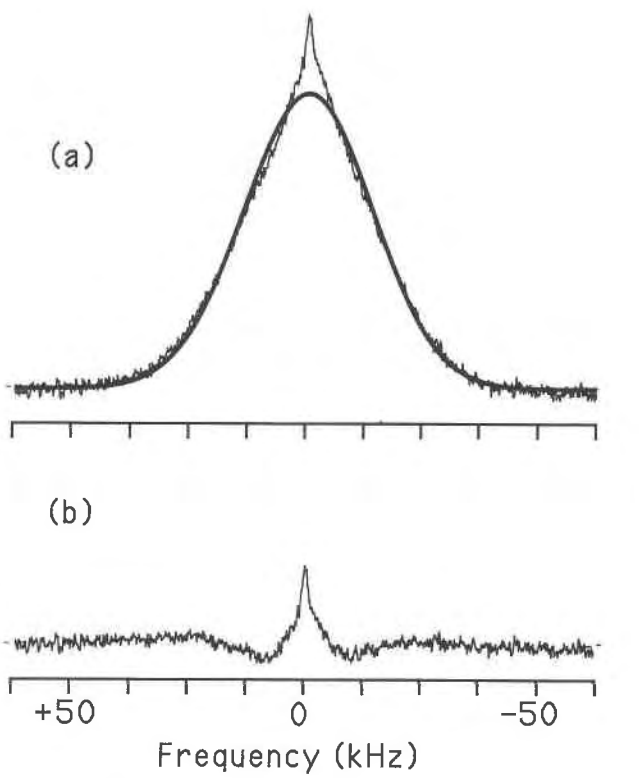

Fig. 10. (**a**) Proton NMR spectrum of the synthetic hydrogarnet powder. The spectrum is the average of 64 scans with a recycle delay of 4 s per scan. The thick black line represents a least-squares fit of a Gaussian function to the experimental line shape. (**b**) Difference of the least-squares fit and the experimental spectrum, plotted on the same vertical scale as (**a**).

NMR line shape analysis

Synthetic hydrogarnet. Detailed microscopic information can be extracted from relatively featureless NMR lines, such as the broad peak in Figure 10, by the method of moments (van Vleck, 1948). Though normally a straightforward numerical exercise, the presence of the overlapped narrow peak complicates the calculation, since the moments of the unwanted signal are superimposed on the moments of the line of interest, i.e., the broad peak. Hence, we have attempted to fit the main peak to various line shapes, and to use the fitted line shape to infer the moments instead of the experimental line shape. Because the second peak is considerably narrower than the main peak, it is feasible to use only regions of the spectrum that lie outside the band width of the second peak in our least-squares fit calculation. The source of the second resonance was not identified but is presumably a H-containing contaminant mixed with the hydrogarnet powder.

The function that was found empirically to give the best fit to the spectrum was the normalized Gaussian function:

$$F(\nu) = \frac{1}{a} e^{-\pi\left(\frac{\nu-\nu_0}{a}\right)^2}, \quad (4)$$

The second moment of this function is

$$M_{2,\,\text{Gaussian}} = \frac{a^2}{2\pi}. \tag{5}$$

The plot of the fitted spectrum and the experimental spectrum reveals the Gaussian to be a close representation of the broad line shape.

Expressions for the second moment of dipolar coupled-spin ½ nuclei have been derived from first principles for comparison with experimentally measured second moments. For samples that contain proton clusters with an isotropic continuum of orientations, such as powders and crystals with complex unit cells, the second moment of the NMR line shape in the absence of chemical shifts is, in units of Hertz squared (Abragam, 1961):

$$M_2 = \frac{1}{4\pi^2}\frac{3}{5}\gamma^4\hbar^2 I(I+1)\sum_{k=2}^{N}\frac{1}{r_{1k}^6} \tag{6}$$

where the r_{1k} are interproton distances, I is the spin quantum number (in this case, ½), γ is the gyromagnetic ratio of the isotope in radians per second, and N is the number of magnetically coupled spins, which, in theory, could include every H nucleus within the crystallite. The multiple-quantum NMR results on this sample demonstrate, however, that it is valid to regard the $(OH)_4$ tetrahedra in the hydrogarnet powder as very nearly isolated clusters of four H nuclei in a proton NMR measurement. We shall assume, therefore, that the NMR spectrum of the hydrogarnet is an orientationally averaged superposition of spectra of tetrahedral H clusters, and that $N = 4$. If we suppose that the protons of the four spin $(OH)_4$ cluster lie at the vertices of a regular tetrahedron, M_2 reduces to

$$M_2 = \frac{1}{4\pi^2}\frac{27}{20}\frac{\gamma^4\hbar^2}{r_t^6} \tag{7}$$

where r_t is the interproton separation.

From the fit of the Gaussian to the hydrogarnet powder NMR spectrum, a value for M_2 can be estimated; this value was determined to be $M_{2,\,\text{exp}} = 1.917 \times 10^8$ Hz^2. Taking this to be the value of M_2 in Equation 7 above and solving for r_t, we discover $r_t = 2.16$ Å.

Inasmuch as the line width of the experimental spectrum contains contributions from sources other than the homonuclear dipolar coupling, such as paramagnetic broadening, chemical shift anisotropy, and heteronuclear couplings to ^{27}Al and ^{29}Si nuclei, the second moment actually attributable to the H-H dipolar coupling will be somewhat less than $M_{2,\,\text{exp}}$. For this reason, our value of r_t is best regarded as a lower limit for the true dimension of the $(OH)_4$ tetrahedron.

The configuration of the H nuclei in the hydrogarnet $(OH)_4$ tetrahedron has been previously determined by X-ray methods (Foreman, 1968). According to these results, the tetrahedron formed by the four nuclei is distorted, with two characteristic interproton distances of 1.82 and 2.42 Å instead of one. The single distance we have found lies close to the mean of these two values.

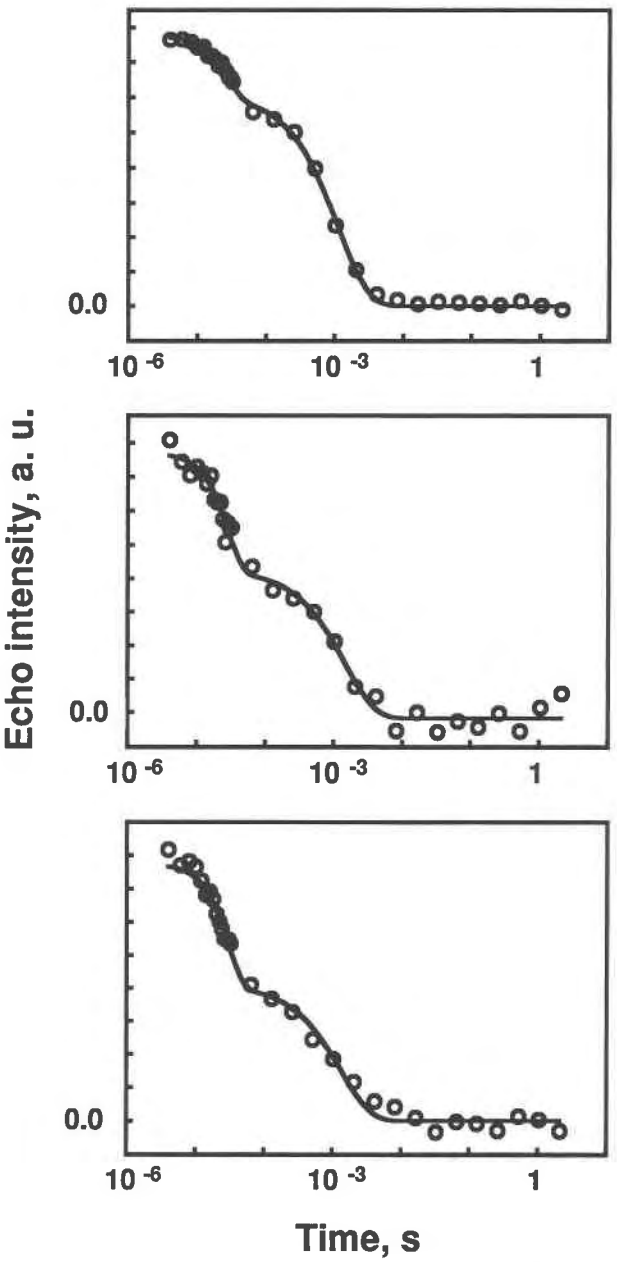

Fig. 11. Decay of the solid echo amplitude as a function of the logarithm of the refocusing time for the Tanzanian grossular garnet (**top**), the colorless grossular garnet specimen from the Jeffrey quarry, Asbestos, Quebec (**middle**), and the orange grossular specimen from Asbestos, Quebec (**bottom**). The circles are experimental data, the line a least-squares fit of Eq. 8 to the data. Each experimental point was obtained from the sum of 256 spin-lock transients of 4096 complex points each, with a recycle delay per scan of 4 s.

Grossular garnet single crystals. An accurate determination of pair interproton distances by a line shape moment analysis requires that we be able to separate the contribution to the line width of short-range homonuclear dipolar couplings from contributions due to other

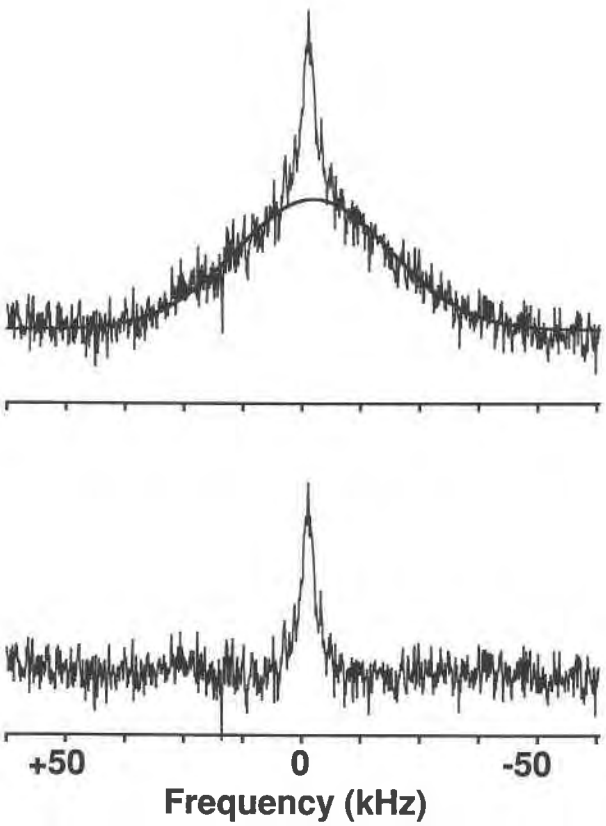

Fig. 12. (**Top**) Proton NMR spectrum of the Tanzanian garnet single crystal. The spectrum is the average of 2000 scans with a 4-s delay between scans. The bold line is a least-squares fit of a Gaussian line shape to the experimental spectrum. (**Bottom**) Difference of the least-squares fit spectrum and the experimental spectrum plotted on the same vertical scale as the top spectrum.

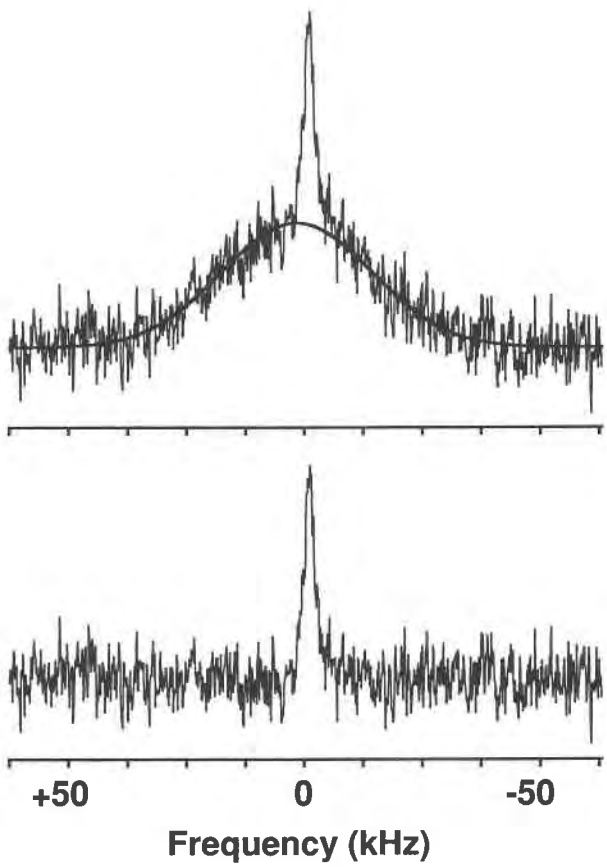

Fig. 13. Same as Fig. 12, but for the colorless grossular specimen from the Jeffrey quarry, Asbestos, Quebec.

line broadening sources. This separation can be approximately effected by means of a procedure developed by Boden et al. (1974, 1975), Boden and Mortimer (1973), Boden and Levine (1975, 1978), and Boden and Kahol (1983), based on measurements of the solid echo envelope decay (SEED). This experiment, shown in Figure 1d, was performed on all three grossular single crystals, with the results summarized by Figure 11. These data were fitted to a sum of one Gaussian function and one exponential function of the form

$$f(t) = A_0 - A_1 e^{-\pi(t/\tau_{\mathrm{Gau}})^2} - A_2 e^{-t/\tau_{\mathrm{exp}}}. \quad (8)$$

Significantly worse correlations were obtained by attempts to fit the data to two Gaussians or two exponentials.

Table 2. Spin echo envelope decay time constants

Sample	τ_{Gau} (s)	τ_{exp} (s)
Tanzanian grossular	4.904×10^{-5}	1.156×10^{-3}
Colorless grossular, Jeffrey quarry, Asbestos, Quebec	5.068×10^{-5}	1.474×10^{-3}
Orange grossular, Asbestos, Quebec	5.307×10^{-5}	1.332×10^{-3}

Values for the decay time constants τ_{Gau} and τ_{exp} are gathered in Table 2. These data and the decay curves of Figure 11 show that the decays of the solid echo envelopes take place in two distinct steps. The possibility that the natural garnet samples contain two chemically distinct types of protons has already been mentioned in the previous discussion of the NMR line shapes. The observation of the two step echo envelope decay appears to affirm this hypothesis.

A second point of interest revealed by these data is that the three decay curves, although superficially very dissimilar, have very nearly the same decay time constants for both the exponential and the Gaussian components of $f(t)$. The meaning of this parallel is not clear but could indicate that two of the same type of proton are indeed present in all three garnet samples, but in varying relative amounts.

Thirdly, we note that τ_{Gau} and τ_{exp} are both considerably larger than the T_2 measured from the line widths of each of the samples. The implications of this observation will be explored later in this section, but for now we note that the discrepancy provides a measure of the size of line

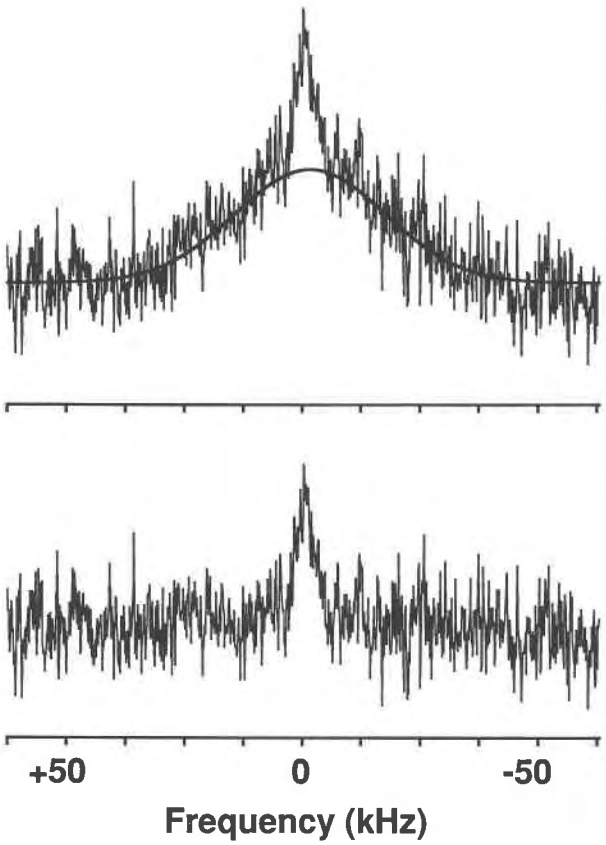

Fig. 14. Same as Fig. 12, but for the orange grossular specimen from Asbestos, Quebec.

broadening interactions exclusive of the intrapair homonuclear dipolar couplings.

The fourth interesting feature in these data is the exponential behavior of the slower decay process. The Fourier transform of an exponential decay curve is a Lorentzian function, a line shape function that is often symptomatic of a highly mobile species or nuclear spins that are very weakly coupled by magnetic interactions to other spins around them (Abragam, 1961). Further work, such as a variable temperature study, is necessary before we can make a more definite interpretation of this result.

The evidence presented thus far indicates that H nuclei in the grossular garnets are incorporated in the crystal in at least two distinct forms. The broad line and the narrow line in the spectra of Figures 2–4 presumably correspond to these two species. Assuming that to be the case, the relative areas of the two NMR lines provide a measure of the relative amounts of the two species. For the purposes of computing these areas, we are helped by the large disparity in line widths, which enables us to fit the broad resonance to some model line shape function using parts of the spectrum that contain little or no intensity contribution from the narrow peak. Since the narrow peak constitutes such a small fraction of the total spectral width, very few points need actually be excluded from the fit

Table 3. Proton NMR line widths and line area ratios

Sample	Line width, FWHH (kHz)	A_{narrow}/A_{broad}
Synthetic hydrogarnet powder	32.60	na
Tanzanian grossular	39.56 ± 0.89	0.155 ± 0.052
Colorless grossular, Jeffrey quarry, Asbestos, Quebec	37.06 ± 0.34	0.124 ± 0.034
Orange grossular, Asbestos, Quebec	37.32 ± 0.61	0.172 ± 0.015

Note: errors are standard deviations computed from three measurements of each quantity.

calculation to excise the narrow peak. The function thus fitted to the broad resonance may then be subtracted from the experimental spectrum and the area of the narrow peak evaluated numerically for comparison with the integral of the fitted function.

The outcome of this procedure is shown in Figures 12, 13, and 14. The line shape function that agrees best with the data is the Gaussian function in Equation 4, with a full width at half height of

$$\Delta\nu_{1/2} = 2a\left[-\frac{1}{\pi}\ln\left(\frac{1}{2}\right)\right]^{1/2}. \quad (9)$$

The flatness of the base line proves the close correspondence of the fitted Gaussian to the shape of the broad resonance.

The line widths of the broad peak (as calculated with the Gaussian model) and the ratios of the area of the narrow peak to the broad peak are shown in Table 3. The values presented are averages computed from three fitted spectra per sample, measured for three orientations of each crystal. The line widths of the three grossular specimens are very similar to one another, but differ significantly from the line width of the hydrogarnet powder spectrum. Moreover, the ratios of narrow to broad areas nearly coincide. The line shapes of the narrow peaks differ markedly, however, as may be seen in Figure 15.

The chemical identity of the H nuclei corresponding to the narrow peak cannot be ascertained on the basis of the available NMR data. The narrow width of this line and the echo envelope decay results both indicate that the H nuclei are either far removed from other H nuclei or are part of a mobile species within the sample.

We have proposed on the basis of the multiple-quantum NMR spectra that H nuclei are grouped pairwise in the Tanzanian grossular. If we assume that the interproton vector of the H pair can point in any direction in a single crystal with equal probability, then the contribution to the second moment due solely to the intrapair dipolar interaction is

$$M_{2,\,\mathrm{intra}} = \frac{1}{4\pi^2}\frac{9}{20}\frac{\gamma^4\hbar^2}{R^6}. \quad (10)$$

This equation contains, besides the assumption of equiprobable H pair orientations, the second significant assumption, that all paired H nuclei are separated from their partners by the same distance, R.

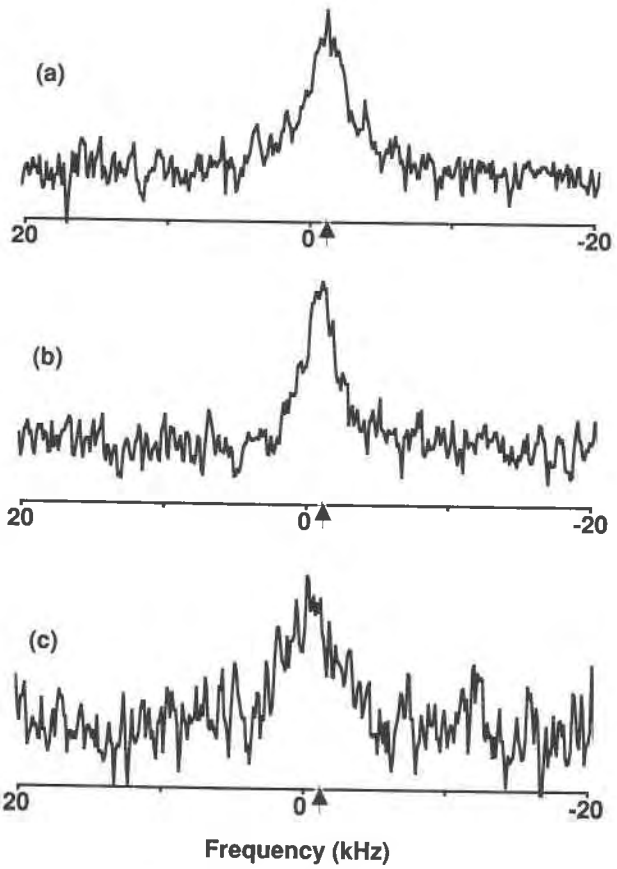

Fig. 15. Difference spectra of Figs. 12, 13, and 14 on an expanded frequency axis. (**a**) Tanzanian grossular, (**b**) colorless grossular from the Jeffrey quarry, Asbestos, Quebec, (**c**) orange grossular from Asbestos, Quebec. The position of the TMS chemical shift standard is designated by the arrows.

In addition to intrapair dipolar couplings, NMR lines can be broadened by interactions about which little may be known, such as heteronuclear couplings, chemical shift anisotropies, and interpair homonuclear dipolar couplings. The cumulative effect of these additional sources of line broadening can be represented mathematically as a quantity $M_{2,\,\text{other}}$, which must be added to $M_{2,\,\text{intra}}$ to obtain the measured second moment:

$$M_2 = M_{2,\,\text{intra}} + M_{2,\,\text{other}}. \qquad (11)$$

In this equation, M_2 is the second moment computed directly from the observed NMR line, and $M_{2,\,\text{intra}}$ is the quantity defined in Equation 10.

Table 4. Second moments

Sample	$M_{2,\text{exp}}$ (Hz^2)	$M_{2,\text{SEED}}$ (Hz^2)	$M_{2,\text{intra}}$ (Hz^2)
Tanzanian grossular	2.823×10^8	0.662×10^8	2.161×10^8
Colorless grossular, Jeffrey quarry, Asbestos, Quebec	2.477×10^8	0.612×10^8	1.865×10^8
Orange grossular, Asbestos, Quebec	2.511×10^8	0.565×10^8	1.946×10^8

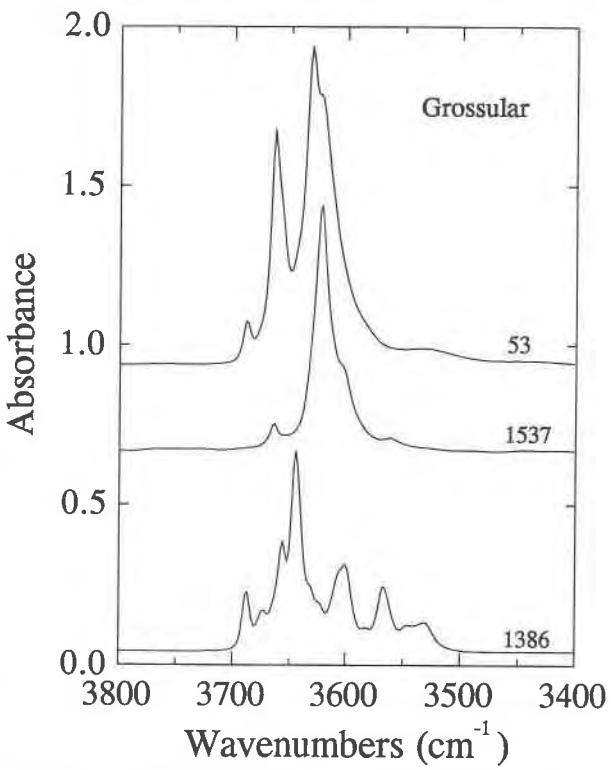

Fig. 16. Infrared absorption spectra in the OH-stretching region of single-crystal grossular garnets plotted as 1.00 mm in thickness. From top to bottom: pale orange from Asbestos, Quebec; colorless from Jeffrey mine, Quebec; colorless from Lelatema Hills, Kenya.

A method for accomplishing the separation of second moments has been developed by Boden et al. (1974, 1975), Boden and Mortimer (1973), Boden and Levine (1975, 1978), and Boden and Kahol (1983), and demonstrated on model two-spin and heteronuclear systems. Strictly speaking, none of the special cases treated by them contains simultaneously the full range of magnetic interactions potentially present in the Tanzanian garnet. Nevertheless, their theory is readily generalized to handle other situations, and no significant modifications of their analysis become necessary when applying their procedures to the Tanzanian garnet.

According to the generalized analysis of the echo envelope decay, the line obtained by Fourier transformation of the spin echo envelope has a second moment $M_{2,\,\text{SEED}}$, which can be shown to equal

$$M_{2,\,\text{SEED}} = M_{2,\,\text{other}}. \qquad (12)$$

The measurement of $M_{2,\,\text{SEED}}$, therefore, offers the means for determining $M_{2,\,\text{intra}}$ by Equation 11.

We have analyzed echo envelope decays as prescribed by this generalized method to obtain estimates for the values of $M_{2,\,\text{other}}$ and $M_{2,\,\text{intra}}$. The echo envelope decay curves pictured with fits in Figure 11 all show two overlapping lines after Fourier transformation, one a broad Gaussian and one a narrower Lorentzian.

Second moments computed from both the NMR spectra and the echo envelope decay curves through Equation 5 are exhibited in Table 4. $M_{2,\text{intra}}$ has been calculated from $M_{2,\text{SEED}}$ and M_2 through the use of Equations 11 and 12. Inserting $M_{2,\text{intra}}$ for the Tanzanian garnet into Equation 10 and solving for R, we find $R = 1.76$ Å. If instead we use M_2 to solve for R, we obtain the slightly smaller value $R = 1.69$ Å. For comparison, we observe that interproton distances in crystalline H_2O molecules have been measured by NMR for a number of inorganic hydrates and have been found to lie in the range $1.58 \leq R_{H\text{-}H} \leq 1.62$ Å (Pake, 1948; Weitekamp et al., 1983; Keller, 1988).

We note in closing that as a practical matter the Fourier transform of the echo envelope decay curve need not be actually computed in order to obtain $M_{2,\text{SEED}}$, as suggested by the previous discussion; with the presumption that the echo envelope decay follows a Gaussian function, the second moment may instead be calculated from the Gaussian fit parameters through Equation 5. The echo envelope decay moments measured in this work were in fact derived in this way.

Comparison with infrared data

The three single-crystal grossular samples exhibit different types of IR spectroscopic behavior in the OH stretching region. The spectrum of the Tanzanian grossular (1386), with a complex pattern of at least 12 OH stretches (Fig. 16), is similar to the spectrum of grossular 771, suggesting that its modes of OH incorporation are more complex than the hydrogrossular substitution (Rossman and Aines, 1991). The corresponding NMR result indicating that protons are clustered in pairs is supportive of this conclusion.

The infrared spectrum of the colorless Canadian grossular (1537) is a class 4 spectrum in the scheme of Rossman and Aines, which, among the samples suitable for the NMR experiment, most closely resembles that of the synthetic hydrogrossular and, by inference, is the one most likely to contain H in the hydrogarnet substitution. It was chosen because it is the garnet that has the fewest spectroscopic components in addition to the dominant 3621 cm^{-1} band. The indication of protons clustered in groups of four from the multiple-quantum spectra are consistent with the interpretation of the IR spectra. Additional weak features in the IR spectrum could represent the protons in clusters of size two indicated by the NMR results.

The pale orange grossular from Canada (53) contains both the features of the colorless sample (1537) plus prominent added features at 3631 and 3664 cm^{-1} in the spectrum, suggesting that multiple OH sites could be present.

Acknowledgments

Samples used in these experiments were generously provided by P. Flusser (Overland Gems, Los Angeles), R.D. Shannon (E.I. DuPont), and G.A. Lager (University of Louisville). H.C. thanks D.P. Weitekamp and D.N. Shykind for helpful discussions and their interest in this work. Primary funding for this project was provided by the White Rose Foundation, whose assistance is greatly appreciated. Additional funding for spectrometer time was obtained from NSF grant EAR-89-16064. Pacific Northwest Laboratory is operated for the U.S. Department of Energy by Battelle Memorial Institute under contract DE-AC06-76RLO 1830.

References cited

Abragam, A. (1961) Principles of nuclear magnetism, p. 1–599. Clarendon, Oxford, England.

Basso, R., and Cabella, R. (1990) Crystal chemical study of garnets from metarodingites in the Voltri Group metaophilites (Ligurian Alps, Italy). Neues Jahrbuch für Mineralogie Monatshefte, 127–136.

Baum, J., and Pines, A. (1986) NMR studies of clustering in solids. Journal of the American Chemical Society, 108, 7447–7454.

Baum, J., Munowitz, M., Garroway, A.N., and Pines, A. (1985) Multiple-quantum dynamics in solid state NMR. Journal of Chemical Physics, 83, 2015–2025.

Birkett, T.C., and Trzcienski, W.E. (1984) Hydrogarnet: Multi-site hydrogen occupancy in the garnet structure. Canadian Mineralogist, 22, 675–680.

Boden, N., and Kahol, P.K. (1983) NMR solid echoes in systems of coupled pairs of spin-½. I. Theoretical model. Molecular Physics, 50, 645–665.

Boden, N., and Levine, Y.K. (1975) Interpair dipolar interactions in solids containing spin-½ pairs. Molecular Physics, 29, 1221–1227.

——— (1978) Calculation of NMR spin echo responses in solids. Journal of Magnetic Resonance, 30, 327–342.

Boden, N., and Mortimer, M. (1973) An NMR "solid" echo experiment for the direct measurement of the dipolar interactions between spin-½ pairs in solids. Chemical Physics Letters, 21, 538–540.

Boden, N., Gibb, M., Levine, Y.K., and Mortimer, M. (1974) Spin-echo experiments for determination of the homo- and heteronuclear contributions to the van Vleck moments of NMR absorption spectra in solids. Journal of Magnetic Resonance, 16, 471–482.

Boden, N., Levine, Y.K., Lightowlers, D., and Squires, R.T. (1975) NMR dipolar echoes in solids containing spin-½ pairs. Molecular Physics, 29, 1877–1891.

Burum, D.P., Linder, M., and Ernst, R.R. (1981) A new "tune-up" NMR pulse cycle for minimizing and characterizing phase transients. Journal of Magnetic Resonance, 43, 463–471.

Cohen-Addad, C., Ducros, P., and Bertaut, E.F. (1967) Etude de la substitution du groupement SiO_4 par $(OH)_4$ dans les composés $Al_2Ca_3(OH)_{12}$ et $Al_2Ca_3(SiO_4)_{2.16}(OH)_{3.36}$ de type grenat. Acta Crystallographica, 23, 220–230.

Foreman, Jr., D.W. (1968) Neutron and x-ray diffraction study of $Ca_3Al_2(O_4D_4)_3$, a garnetoid. Journal of Chemical Physics, 48, 3037–3041.

Freeman, R., Frenkiel, T.A., and Levitt, M.H. (1981) Composite z-pulses. Journal of Magnetic Resonance, 44, 409–412.

Hoffman, R.A. (1970) Lineshapes in high resolution NMR. In J.S. Waugh, Ed., Advances in magnetic resonance, vol. 4, p. 87–200. Academic, New York.

Kalinichenko, A.M., Proshko, V.Ya., Matyash, I.V., Pavlishin, V.I., and Gamarnik, M.Ya. (1987) Geochemistry international, 24, 132–135 (translated from Geokhimiya, 9, 1363–1366, 1986.)

Keller, A. (1988) Spin-1 behaviour of systems of dipolar coupled pairs of spin-½ nuclei. In W.S. Warren, Ed., Advances in magnetic resonance, vol. 12, p. 183–246. Academic, New York.

Lager, G.A., Armbruster, T., and Faber, J. (1987) Neutron and x-ray diffraction study of hydrogarnet $Ca_3Al_2(O_4H_4)$. American Mineralogist, 72, 756–765.

Mehring, M. (1983) Principles of high resolution NMR in solids, p. 295–304. Springer-Verlag, Berlin.

Messiah, A. (1976) Quantum mechanics, p. 664–679. Wiley, New York.

Munowitz, M., and Pines, A. (1987) Principles and applications of multiple-quantum NMR. In I. Prigogine and S.A. Rice, Eds., Advances in chemical physics, vol. LXVI, p. 1–152. Wiley Interscience, New York.

Novak, G.A., and Gibbs, G.V. (1971) The crystal chemistry of silicate garnets. American Mineralogist, 56, 791–825.

Ostroff, E.D., and Waugh, J.S. (1966) Multiple spin echoes and spin locking in solids. Physical Review Letters, 16, 1097–1098.

Pake, G.E. (1948) Nuclear resonance absorption in hydrated crystals: Fine structure of the proton line. Journal of Chemical Physics, 16, 327–336.
Powles, J.G., and Strange, J.H. (1963) Zero time resolution nuclear magnetic resonance (NMR) transients in solids. Proceedings of the Physical Society, London, 82, 6–15.
Rhim, W.-K., Burum, D.P., and Elleman, D.D. (1976) Multiple-pulse spin-locking in dipolar solids. Physical Review Letters, 37, 1764–1769.
Rossman, G.R., and Aines, R.D. (1991) The hydrous components in garnets: Grossular-hydrogrossular. American Mineralogist, 76, 1153–1164.
Shannon, R.D., and Rossman, G.R. (1992) Dielectric constants of silicate garnets and the oxide additivity rule. American Mineralogist, 77, 94–100.
Skykind, D.N., Baum, J., Liu, S.-B., Pines, A., and Garroway, A.N. (1988) Phase-incremented multiple-quantum NMR experiments. Journal of Magnetic Resonance, 76, 149–154.
Suter, D., Liu, S.-B, Baum, J., and Pines, A. (1987) Multiple-quantum NMR excitation with a one-quantum Hamiltonian. Chemical Physics Letters, 114, 103–109.
van Vleck, J.H. (1948) The dipolar broadening of magnetic resonance lines in crystals. Journal of Chemical Physics, 74, 1168–1183.
Warren, W.S., Weitekamp, D.P., and Pines, A. (1980) Theory of selective excitation of multiple-quantum transitions. Journal of Chemical Physics, 73, 2084–2099.
Weitekamp, D.P. (1983) Time domain multiple-quantum NMR. In J.S. Waugh, Ed., Advances in magnetic resonance, vol. 11, p. 111–274. Academic, New York.
Weitekamp, D.P., Bielecki, A., Zax, D.B., Zilm, K., and Pines, A. (1983) Zero-field nuclear magnetic resonance. Physical Review Letters, 50, 1807–1810.
Wokaun, A., and Ernst, R.R. (1978) The use of multiple-quantum transitions for relaxation studies in coupled spin systems. Molecular Physics, 36, 317–341.
Yesinowski, J.P., Eckert, H., and Rossman, G.R. (1988) Characterization of hydrous species in minerals by high speed ^{1}H MAS-NMR. Journal of the American Chemical Society, 110, 1367–1375.

Manuscript received February 22, 1993
Manuscript accepted July 27, 1993

Appendix 1.

This appendix presents a derivation of an a priori limit on the maximum multiple-quantum transition order that can be observed in the nonselective multiple-quantum experiment described in the experimental section. One upper limit can be deduced immediately: a cluster of N spin ½ nuclei can absorb or emit no more than N photons in a single multiple-quantum transition. The observed maximum can often be less, however, depending on the details of the experiment and on physical properties unique to the spin cluster under investigation. Here we shall demonstrate that for an N spin ½ cluster, the $\pm N$ quantum lines are not observable in the nonselective multiple-quantum experiment of Suter et al. (1987) and confirm the assertion made earlier that a multiple-quantum spectrum manifesting only ± 1 quantum lines is indicative of a proton cluster of size $N \geq 2$.

The multiple-quantum NMR experiment utilized in this work consists of a sequence of events that can be divided into four distinct time intervals, viz., the preparation, evolution, mixing, and detection periods. The multiple-quantum interferogram recorded in such an experiment can be calculated from the general expression

$$S(\tau_p, \tau_m, x_1) = \mathrm{Tr}[DU_m(\tau_m)U_E(x_1)U_p(\tau_p)\rho_0 U_p^\dagger(\tau_p) \cdot U_E^\dagger(x_1)U_m^\dagger(\tau_m)]. \quad \text{(A1)}$$

(Weitekamp, 1983; Munowitz and Pines, 1987). In the above equation, τ_m and τ_p are the durations of the mixing and preparation periods, respectively, x_1 is some quantity such as time or radio frequency phase that is incremented from acquisition to acquisition during the experiment (usually, but not exclusively, in the evolution period), D is the quantum-mechanical operator corresponding to the detected observable, ρ_0 is the nuclear spin density operator at the start of the experiment, and $U_m(\tau_m)$, $U_E(x_1)$, and $U_p(\tau_p)$ are the unitary evolution operators describing the time development of the spin system during the mixing, evolution, and preparation periods, respectively. If we cyclically permute the order of multiplication of the matrices on the right side of Equation A1 (which leaves the trace invariant) and expand the expression in some complete orthonormal basis, we arrive at the equation

$$\begin{aligned} S(\tau_p, \tau_m, x_1) &= \mathrm{Tr}\{[U_E^\dagger(x_1)U_m^\dagger(\tau_m)DU_m(\tau_m)U_E(x_1)] \cdot [U_p(\tau_p)\rho_0 U_p^\dagger(\tau_p)]\} \\ &= \sum_{j,k} \langle j|D'(\tau_m, x_1)|k\rangle\langle k|\rho_0'(\tau_p)|j\rangle \quad \text{(A2)} \end{aligned}$$

where $D'(\tau_m, x_1)$ and $\rho_0'(\tau_p)$ are defined by the Hermitian operators

$$D'(\tau_m, x_1) \equiv U_E^\dagger(x_1)U_m^\dagger(\tau_m)DU_m(\tau_m)U_E(x_1) \quad \text{(A3)}$$

$$\rho_0'(\tau_p) \equiv U_p(\tau_p)\rho_0 U_p^\dagger(\tau_p). \quad \text{(A4)}$$

Since the answer will be independent of the basis in which the trace expression is evaluated, we can choose an orthonormal basis which has as two of its basis vectors the Zeeman eigenstates $|\pm N/2\rangle$, corresponding to the product states in which all N spins are in the $+½$ and $-½$ eigenstates of the I_z spin operator, respectively. In this basis, the entire $\pm N$ quantum amplitude of the detected multiple-quantum signal is mathematically contained in just two terms in the expansion of Equation A2, specifically:

$$S_{+N}(\tau_p, \tau_m, x_1) = \langle N/2|D'(\tau_m, x_1)|-N/2\rangle \cdot \langle -N/2|\rho_0'(\tau_p)|N/2\rangle \quad \text{(A5)}$$

and

$$S_{-N}(\tau_p, \tau_m, x_1) = \langle -N/2|D'(\tau_m, x_1)|N/2\rangle \cdot \langle N/2|\rho_0'(\tau_p)|-N/2\rangle. \quad \text{(A6)}$$

Note that because of the hermiticity of $D'(\tau_m, x_1)$ and $\rho_0'(\tau_p)$, we have

$$S_{+N}(\tau_p, \tau_m, x_1) = [S_{-N}(\tau_p, \tau_m, x_1)]^* \quad \text{(A7)}$$

where the asterisk symbolizes the complex conjugate.

The task of proving that the $\pm N$ quantum transitions are not observable in the nonselective multiple-quantum

experiment therefore reduces to a demonstration of the equality

$$S_{+N}(\tau_p, \tau_m, x_1) = 0. \tag{A8}$$

To prove this statement, we shall explicitly evaluate the matrix element $\langle -N/2|\rho_0'(\tau_p)|N/2\rangle$ and show that it is identically equal to zero.

A proof of this equality based on the symmetry of time reversal (Messiah, 1976) may be formulated in the following way. The quantum mechanical time reversal operator, which we designate by the symbol $\mathcal{T}$, can be regarded as the product of two operators, as below:

$$\mathcal{T} = \mathcal{Y}K \tag{A9}$$

where K is the operator that transforms wave functions into their complex conjugates, and $\mathcal{Y}$ is the rotation operator:

$$\mathcal{Y} = e^{-i\pi I_y}. \tag{A10}$$

The inverse of $\mathcal{T}$ has the form

$$\mathcal{T}^\dagger = K\mathcal{Y}^\dagger. \tag{A11}$$

We proceed to make use of this symmetry operation by evaluating the $(-N/2, N/2)$ element of $\rho_0'(\tau_p)$:

$$\begin{aligned}
&\langle -N/2|\rho_0'(\tau_p)|N/2\rangle \\
&\quad = \langle -N/2|U_p(\tau_p)\rho_0 U_p^\dagger(\tau_p)|N/2\rangle \\
&\quad = \langle -N/2|\{\mathcal{T}^\dagger\mathcal{T}U_p(\tau_p)\mathcal{T}^\dagger\mathcal{T}\rho_0\mathcal{T}^\dagger\mathcal{T}U_p^\dagger(\tau_p)\mathcal{T}^\dagger\mathcal{T}|N/2\rangle\} \\
&\quad = \langle -N/2|\{\mathcal{T}^\dagger[\mathcal{T}U_p(\tau_p)\mathcal{T}^\dagger][\mathcal{T}\rho_0\mathcal{T}^\dagger][\mathcal{T}U_p^\dagger(\tau_p)\mathcal{T}^\dagger] \\
&\qquad \cdot\mathcal{T}|N/2\rangle\}
\end{aligned} \tag{A12}$$

where we have made use of the equality $\mathbf{1} = \mathcal{T}^\dagger\mathcal{T}$, with $\mathbf{1}$ the identity operator.

The initial density operator ρ_0 in all of the multiple-quantum NMR experiments of this work was the reduced high-field equilibrium density operator, i.e., an operator that is proportional to the spin angular momentum operator I_z. This fact, combined with the definition of $\mathcal{T}$, gives us the equality

$$\mathcal{T}\rho_0\mathcal{T}^\dagger = -\rho_0. \tag{A13}$$

In the multiple-quantum experiment that concerns us here, the time development operator of the preparation period is well approximated by the unitary propagator:

$$U_p(\tau_p) = e^{-i\mathcal{H}_{xz}\tau_p} \tag{A14}$$

where

$$\mathcal{H}_{xz} = \sum_{\substack{j,k \\ j>k}} d'_{jk}(I_{zj}I_{xk} + I_{xj}I_{zk}). \tag{A15}$$

Since the effective preparation Hamiltonian $\mathcal{H}_{xz}$ is purely bilinear in spin operators, then

$$\mathcal{T}\mathcal{H}_{xz}\mathcal{T}^\dagger = \mathcal{H}_{xz} \tag{A16}$$

which allows us to write

$$\begin{aligned}
\mathcal{T}U_p(\tau_p)\mathcal{T}^\dagger &= e^{-\tau_p(\mathcal{T}i\mathcal{H}_{xz}\mathcal{T}^\dagger)} \\
&= e^{+i\mathcal{H}_{xz}\tau_p} \\
&= U_p^\dagger(\tau_p).
\end{aligned} \tag{A17}$$

To complete this simplication of Equation A12, we recall from our definition of $\mathcal{T}$ that the time-reversed wavefunctions will have the form

$$\mathcal{T}|N/2\rangle = (-1)^N|\ -N/2\rangle \tag{A18}$$

and

$$\langle -N/2|\mathcal{T}^\dagger = \langle N/2|. \tag{A19}$$

The minus sign on the right of Equation (A18) is a consequence of the fact that the eigenfunctions of a spin ½ particle are spinors.

Combining Equations A13, A17, A18, and A19 and utilizing the known properties of the time reversal operator, we obtain:

$$\begin{aligned}
&\langle -N/2|\rho_0'(\tau_p)|N/2\rangle \\
&\quad = (-1)^{N+1}\langle -N/2|[\mathcal{T}^\dagger U_p^\dagger(\tau_p)\rho_0 U_p(\tau_p)|\ -N/2\rangle] \\
&\quad = (-1)^{N+1}\{[\langle -N/2|\mathcal{T}^\dagger] \\
&\qquad \cdot[U_p^\dagger(\tau_p)\rho_0 U_p(\tau_p)|\ -N/2\rangle]\}^* \\
&\quad = (-1)^{N+1}[\langle N/2|U_p^\dagger(\tau_p)\rho_0 U_p(\tau_p)|\ -N/2\rangle]^*.
\end{aligned} \tag{A20}$$

The hermiticity of ρ_0 and the unitarity of $U_p(\tau_p)$ imply that the last expression above can be written

$$\begin{aligned}
&\langle -N/2|\rho_0'(\tau_p)|N/2\rangle \\
&\quad = (-1)^{N+1}\langle -N/2|U_p^\dagger(\tau_p)\rho_0 U_p(\tau_p)|N/2\rangle.
\end{aligned} \tag{A21}$$

An alternative expression for the matrix element on the left side may be derived by writing the identity operator as

$$\mathbf{1} = Z^\dagger Z \tag{A22}$$

with Z defined as the rotation operator:

$$Z \equiv e^{-i\pi I_z}. \tag{A23}$$

Inserting this form for $\mathbf{1}$ into $\langle N/2|\rho_0'(\tau_p)|N/2\rangle$, we see

$$\begin{aligned}
&\langle -N/2|\rho_0'(\tau_p)|N/2\rangle \\
&\quad = \langle -N/2|Z^\dagger[ZU_p(\tau_p)Z^\dagger][Z\rho_0 Z^\dagger][ZU_p^\dagger(\tau_p)Z^\dagger] \\
&\qquad \cdot Z|N/2\rangle.
\end{aligned} \tag{A24}$$

This expression may be reduced by observing that, since ρ_0 is proportional to I_z, then

$$[Z, \rho_0] = 0 \tag{A25}$$

so that

$$Z\rho_0 Z^\dagger = \rho_0. \tag{A26}$$

Furthermore, we observe that

$$\mathcal{Z}\mathcal{H}_{xz}\mathcal{Z}^{\dagger} = -\mathcal{H}_{xz} \tag{A27}$$

from which it follows that

$$\mathcal{Z}U_p(\tau_p)\mathcal{Z}^{\dagger} = U_p^{\dagger}(\tau_p). \tag{A28}$$

Finally, the fact that $|N/2\rangle$ and $|-N/2\rangle$ are, by construction, eigenstates of I_z with eigenvalues $N/2$ and $-N/2$, respectively, enables us to deduce

$$\mathcal{Z}|N/2\rangle = e^{-iN\pi/2}|N/2\rangle \tag{A29}$$

and

$$\langle -N/2|\mathcal{Z}^{\dagger} = \langle -N/2|e^{-iN\pi/2}. \tag{A30}$$

Substituting Equations A26, A28, A29, and A30 into Equation A24 leads to the final result:

$$\langle -N/2|\rho_0'(\tau_p)|N/2\rangle = (-1)^N\langle -N/2|U_p^{\dagger}(\tau_p)\rho_0 U_p(\tau_p)|N/2\rangle. \tag{A31}$$

Comparing Equations A21 and A31, we discover

$$\langle -N/2|\rho_0'(\tau_p)|N/2\rangle = -\langle -N/2|\rho_0'(\tau_p)|N/2\rangle = 0. \tag{A32}$$

We conclude, therefore, that the N quantum transition is not observable in an N spin ½ system if the effective Hamiltonian during the preparation period is of the form $\mathcal{H}_{xz}$ and the initial density operator is proportional to I_z. It follows from this result that a multiple-quantum spectrum measured under these conditions exhibiting only the ± 1-quantum transitions must originate from spin clusters of size $N \geq 2$.

In closing, we note that an analogous time reversal symmetry argument can be constructed to establish more restrictive theoretical limits on the maximum multiple-quantum transition observable for the even-quantum selective version of the multiple-quantum experiment but forgo presenting the proof here.